Author/s:
Tomaskovic-Crook, E;Zhang, P;Ahtiainen, A;Kaisvuo, H;Lee, CY;Beirne, S;Aqrawe, Z;Svirskis, D;Hyttinen, J;Wallace, GG;Travas-Sejdic, J;Crook, JM

Title:
Human Neural Tissues from Neural Stem Cells Using Conductive Biogel and Printed Polymer Microelectrode Arrays for 3D Electrical Stimulation

Date:
2019-08-01

Citation:
Tomaskovic-Crook, E., Zhang, P., Ahtiainen, A., Kaisvuo, H., Lee, C. Y., Beirne, S., Aqrawe, Z., Svirskis, D., Hyttinen, J., Wallace, G. G., Travas-Sejdic, J. & Crook, J. M. (2019). Human Neural Tissues from Neural Stem Cells Using Conductive Biogel and Printed Polymer Microelectrode Arrays for 3D Electrical Stimulation. Advanced Healthcare Materials, 8 (15), https://doi.org/10.1002/adhm.201900425.

DOI: 10.1002/((please add manuscript number))

Article type: Communication

Title: Human Neural Tissues from Neural Stem Cells Using Conductive Biogel and Printed Polymer Microelectrode Arrays for 3D Electrical Stimulation

*Author(s), and Corresponding Author(s)**: Eva Tomaskovic-Crook#, Peikai Zhang#, Annika Ahtiainen, Heidi Kaisvuo, Chong-Yong Lee, Stephen Beirne, Zaid Aqrawe, Darren Svirskis, Jari Hyttinen, Gordon G Wallace, Jadranka Travas-Sejdic*, Jeremy M Crook*

# Eva Tomaskovic-Crook and Peikai Zhang contributed equally to the paper

Dr. E Tomaskovic-Crook, Dr. C-Y Lee, Dr. S Beirne, Prof. G G Wallace, Assoc. Prof. J M Crook

ARC Centre of Excellence for Electromaterials Science, Intelligent Polymer Research Institute, AIIM Facility, University of Wollongong, Australia
E-mail: jcrook@uow.edu.au

Dr. E Tomaskovic-Crook, Assoc. Prof. J M Crook

Illawarra Health and Medical Research Institute, University of Wollongong, Australia

Mr. P Zhang, Prof. J Travas-Sejdic

Polymer Electronics Research Centre, School of Chemical Sciences, The University of Auckland, New Zealand

E-mail: j.travas-sedjic@auckland.ac.nz

Mr. P Zhang, Prof. J Travas-Sejdic

MacDiarmid Institute for Advanced Materials and Nanotechnology, New Zealand

Ms. A Ahtiainen, Ms. H Kaisvuo, Prof. J Hyttinen

Computational Biophysics and Imaging Group, BioMediTech Institute and Faculty of Biomedical Sciences and Engineering, Tampere University of Technology, Tampere, Finland

Dr. Z Aqrawe, Dr. D Svirskis

School of Pharmacy, The University of Auckland, New Zealand

Assoc. Prof. J M Crook

Department of Surgery, St Vincent's Hospital, The University of Melbourne, Australia

Keywords: 3D electrical stimulation; human neural tissue; stem cells; conductive biogel; printed conducting polymer electrodes

Electricity is important in the physiology and development of human tissues such as embryonic and fetal development, and tissue regeneration for wound healing. Accordingly, electrical stimulation (ES) is increasingly being applied to influence cell behaviour and function for a biomimetic approach to *in vitro* cell culture and tissue engineering. Here we describe the application of conductive polymer (CP) poly(3,4-ethylenedioxythiophene)-polystyrenesulfonate (PEDOT:PSS) pillars, direct-write printed in an array format, for three-dimensional (3D) ES of maturing neural tissues that are derived from human neural stem cells (NSCs). NSCs are initially encapsulated within a conductive polysaccharide-based biogel interfaced with the CP pillar (microelectrode) arrays (MEAs), followed by differentiation *in situ* to neurons and supporting neuroglia during stimulation. Electrochemical properties of the pillar electrodes and the biogel support their electrical performance. Remarkably,

stimulated constructs are characterised by widespread tracts of high-density mature neurons and enhanced maturation of functional neural networks. Formation of tissues using the 3D MEAs substantiates the platform for advanced clinically-relevant neural tissue induction, with the system likely amendable to diverse cell types to create other neural and non-neural tissues. The platform may be useful for both research and translation, including modelling tissue development, function and dysfunction, electroceuticals, drug screening and regenerative medicine.

Living cells and tissues exhibit and respond to electrical potentials in the form of naturally occurring bioelectricity, important for tissue development and regeneration, or exogenously delivered electric current *via*, for example, electrodes as medical devices [1-3]. Cellular responses include galvanotaxis [4-6], increased intracellular calcium concentration [7], extracellular matrix assembly [8], and associated cell proliferation and differentiation [1, 7, 9, 10]. Several recent reports have shown that ES can be used to modulate fate determination of differentiating NSCs, including the promotion of neuronal *vs* glial cell induction and increased neuritogenesis [10-12]. From our own research, we have demonstrated the use of biphasic electrical current *via* a conductive polymer, polypyrrole, to promote neurite outgrowth and synaptogenesis of rat primary cortical neurons [13], as well as differentiation of human NSCs to neurons with longer neurites and increased branching, and concomitant lower induction of neuroglia [10].

Human NSCs are native “adult stem cells” that can self-renew, have extended proliferative capacity and retain a multi-lineage potential, being able to differentiate to cells of all neural lineages in the brain. Hence, they may be used for cell-based therapeutics to treat traumatic brain injury and neurological disorders such as epilepsy and Parkinson’s disease, as well as *in vitro* modelling of

neural-development, cell function and dysfunction, and optimisation of medical devices for *in vivo* neural tissue interfacing.

To date, research and development of NSCs, or mammalian cell culture in general, has largely relied upon elementary two-dimensional (2D) methods of cell culture, which are not representative of actual cell environments within tissues and organs of the human body. Therefore, cells cultured as monolayers on flat surfaces and isolated from physiologically relevant inputs, such as electrical potentials, are intrinsically poorly predictive of *in vivo* behaviour, form and function, limiting their value for basic research through to translational use, such as pharmaceuticals development.

The realisation of biomimetic cell culture to better represent human cell growth and tissue outside the human body requires new platforms that integrate biologically relevant human cell lines with advanced techniques for 3D tissue engineering and accordant 3D ES. Here we describe such a platform employed for the *in vitro* development of electrogenic neural tissue using human NSCs (**Figure 1**). The stem cells were derived from human mid-brain, specifically ventral mesencephalon [14], and encapsulated within our previously described clinically-amenable biogel for 3D culture and differentiation [15, 16]. The gel comprises ionically cross-linked alginate (Al), carboxymethyl-chitosan (CMC) and agarose (Ag). Further to our previous reports of the biogels' properties [15-17], we have now electrochemically-characterised the gel to confirm electrical conductivity so as to be favourable for *in situ* cell stimulation. ES of cell-laden gels is achieved using a high resolution direct-write printed array of 3D penetrating CP pillar electrodes for stable and biocompatible cell coupling (**Figure 2**; **Figure S1** and **S2**, Supporting Information) [18]. The 3D multielectrode configuration provides a larger surface area to augment coupling with the developing electrogenic tissue. We have previously described various properties of the CP pillars including surface morphology, as well as

chemical, structural, and mechanical properties [18], however, to the best of our knowledge, our account is the first example of 3D ES of human stem cells *in vitro* to form 3D human tissues, and more specifically functional neural tissues. We submit that the platform is scaleable and versatile, envisioning it being amenable *in vitro* and *in vivo* to neural and non-neural cell and tissue types for stimulation and monitoring applications, with *in vivo* use bolstered by mechanical robustness and flexibility of the pillars to withstand multi-axial mechanical stresses exerted on the pillars.

3D MEAs were fabricated using commercially available Titanium/Au coated microscope slides for photolithographic patterning of individually addressable Au electrodes, onto which PEDOT:PSS-based ink was direct-write printed to form stable CP pillars (Figure S1 and S2a-d, Supporting Information). The height and diameter of the pillars were 80 ± 2 µm and 14 ± 1 µm, respectively, providing a high aspect ratio of ~5.7 for mechanical stability necessary to sustain exposure to cell culture media and the biogel, as well as to support interaction with cells and derivative tissues. Importantly, enclosure of each CP pillar array within a bonded poly(dimethyl siloxane) (PDMS) chamber enabled containment of the cell-laden biogel constructs in culture medium together with a platinum mesh counter electrode to ensure even distribution of ES (Figure 1; Figure S2e-f, Supplementary Information). The mesh was slightly smaller than the PDMS wells' inner dimensions and affixed to a lid that was printed from bio-compatible photo-curable polymer MED610, being positioned above each construct while submerged in the medium (Figure S2f, Supplementary Information).

Electrochemical characterisation of printed CP electrode arrays by cyclic voltammetry (CV) demonstrated well defined electrochemical responses of CP pillars with apparent oxidation and reduction peaks associated with redox active conducting polymer (**Figure 3**a). Importantly, enhanced

conductivity was indicated by a large decrease in impedance for almost the entire tested frequency range after incorporation of CPs (Figure 3b). The calculated cathodic charge storage capacity (CSC_C) increased from 9.5 ± 0.3 mC/cm^2 for Au and 12.1 ± 0.9 mC/cm^2 for CP film to 127 ± 5.6 mC/cm^2 for CP pillars (Figure 3c). Comparison of impedance at 100 Hz for all three electrode types demonstrated a greater than two-orders of magnitude lower impedance of CP pillar electrodes compared to Au electrodes (Figure 3d).

The charge injection limit (CIL) is another important parameter for microelectrodes used for ES, indicating how much current can be applied to each electrode. The applied charge should be within a predetermined limit to avoid irreversible faradic reactions [19]. The CIL was tested by voltage transient measurements (VTM) upon applying a current controlled sub-millisecond stimulation pulse to the electrodes. Similar to CV and impedance performance, the charge injection limit was improved from 0.66 ± 0.05 mC/cm^2 for Au, to 2.31 ± 0.08 mC/cm^2 for CP films, and 11.41 ± 0.46 mC/cm^2 for CP pillars (Figure 3e).

The stability of CP electrodes was initially evaluated by applying intense stimulation and recording impedance. Here we define electrode failure (or delamination) as a 100% change in the impedance at 100 Hz. The CP films delaminated relatively rapidly (estimated at around 1000 pulses; Figure 3f), while the CP pillars were more stable with the average change of impedance magnitude $|Z|$ within 20% at the end of testing after ~10^6 pulses (Figure 3f).

The results of further testing long-term stability of the electrodes within tissue culture media over 19 days are shown in Figure 3g-j. The CV curves of Figure 3g indicate a similar shift of the oxidation peak from -0.3 V on day 1 towards 0 V on day 19 for CP pillar electrodes in Neuro Basal Medium (NBM) and phosphate buffered saline (PBS). However, peak current differs between the

two media, decreasing with time in NBM while remaining stable or even slightly increasing in PBS. The CSC (that is corresponding to the enclosed area of CV) and the more commonly used parameter CSC_C decreased in both media, with the greatest decrease observed in NBM. The CSC_C decreased by 45% in NBM and 35% in PBS, although the final values were similar by day 19 (~47 mC/cm^2; Figure 3h).

Finally, electrochemical impedance spectroscopy (EIS) of electrodes in NBM and PBS provided similar impedance magnitude |Z| *vs* frequency curves (Figure 3i) and the extracted |Z| at 100 Hz (Figure 3j). As expected, the impedance of CP pillars increased with time. This together with the decrease of CSC_C are likely to be related to the influence of water and swelling caused by the hygroscopic PSS [11, 20-22], and the electrode biofouling, where biomolecules present in the culture media adsorb to the electrode surface.

Overall, the CP pillars demonstrated significant reduction in impedance and significant increases in the charge injection limit as well as electrochemical activity in comparison with both flat Au and CP films [23]. These characteristics are likely due to the much higher electrochemical surface area of CP pillars and supported ES using the 3D CP pillars.

A second and critical component of our 3D ES tissue engineering platform is the conductive biogel. Again, electrochemical properties of the gel with and without human NSCs were examined by CV (Figure 3k). Overall, CV demonstrated the gel had well-defined electrochemical responses with or without cells. While biogel in DMEM showed increased capacitance (indicative of increased ionic conductance) compared to DMEM alone, an even larger capacitive current was observed for gel with cells.

Having verified the electrochemical performance of the electrode arrays and biogel, human NSC-laden biogel constructs were prepared for conventional plate-based culture and differentiation as a qualitative point of reference for MEA-based culture. Constructs comprised opaque spheroidal dome structures (diameter: ~5 mm, height: ~1.5 mm) reflecting the polymeric biomaterial encapsulating cells (**Figure 4**a). Immunophenotyping and nuclear-specific staining of NSCs encapsulated within biogels and cultured for 7 days in NSC proliferation medium confirmed the presence of loosely packed NSCs expressing undifferentiated cell markers MKI67 (a marker of cell proliferation, localised to cell nuclei) and intermediate filament protein VIM (Figure 4b). Following culture for 7 days in neural differentiation medium, constructs comprised large numbers of tightly packed cells, with immunocytochemistry and DAPI staining indicating a more heterogeneous distribution of neuronal and glial cells (Figure 4c). More specifically, antibodies for TUBB3 and GFAP revealed early neuronal and to a lesser extent glial cell induction respectively, as well as the morphology of axons and dendritic extensions.

Ensuing assessment of stimulated neural tissue induction and function confirmed the utility of the integrated platform. Firstly, consistent with conventional plate-based culture, gel-laden cells differentiated on the arrays into neurons and glia with or without stimulation (Figure 4d-h). However, while unstimulated constructs were relatively poorly maintained at the interface of the ventral surface of the constructs and the Matrigel-coated insulating layer covering the Au electrodes (Figure 4d), stimulated array-based tissues comprised large numbers of densely packed cells abutting the underlying substrate, with polarised neuronal cells exhibiting axons and dendritic arborisations (Figure 4e). Upon closer examination of stimulated tissues, neurons were observed with axons projecting over long distances from their sites of origin to synapse with other cells including

neuroglia (Figure 4e-inset,f). Synapses and related cellular networking were also signified by axonal swellings, termed varicosities or boutons, formed along the length of individual axons (Figure 4e-inset,f) or as terminal bulbs at the end of an axon (Figure 4f). Notably, in contrast to both conventional tissue induction and unstimulated array-based tissue induction (Figure 4c,g), stimulated tissue was distinguished by more discrete and divergent labelling of neurons expressing TUBB3, MAP2, and presynaptic vesicle glycoprotein SYP. Therefore, confocal z-projection images revealed tracts of intensely labelled and high-density mature MAP2 expressing neurons with SYP; suggestive of structured neuronal network formation and tissue maturation (Figure 4h). Quantitative analyses of TUBB3, MAP2 and SYP immunocytochemistry supported qualitative assessments, with indices of neuronal maturation derived from ratios of mature neuronal MAP2 *vs* immature neuronal TUBB3 ($P < 0.0001$), SYP *vs* TUBB3 ($P < 0.0001$), and SYP *vs* MAP ($P > 0.05$) expression levels, indicating more mature neuronal tissue for stimulated compared to unstimulated samples (Figure 4i; $F(5,54)=18.50$, $P < 0.001$). Furthermore, measures of spatial colocalization of markers determined by correlation analyses based on Pearson's coefficient showed greater colocalization of MAP2 with SYP for stimulated (r=0.748) compared to unstimulated (r=0.595) tissues (Figure 4g-h); consistent with the occurrence of extensive MAP2 and SYP expressing neuronal tracts. A reduced spatial correlation between TUBB3 and SYP was measured for samples with ES (r=0.169) or without ES (r=0.258) (Figure 4g-h).

Finally, cellular networking and function of both unstimulated and stimulated constructs was supported by recurrent spontaneous increases in extracellular calcium concentration (Figure 4j, l). Remarkably, in response to disinhibition of cells by gamma-aminobutyric acid (GABA) receptor-A antagonist bicuculline, stimulated 3D MEA-based cell-laden constructs showed an increased firing

rate and spike amplitude compared to unstimulated constructs (Figure 4k, m). The amplitude of calcium flux was statisically higher for stimulated constructs ($F(3,300)=177.7$, $P < 0.0001$).

In summary, we have shown the neuro-cytocompatibility of the presently described 3D ES tissue engineering platform. Fundamental to the system's performance is the high-resolution 3D printed conducting polymer MEA interfaced with our clinically-amendable electrically conductive biogel. Importantly, the 3D penetrating PEDOT:PSS pillar electrodes demonstrated appropriate activity, resistance, and charge tolerance necessary for ES of biological samples. Moreover, the electrodes are stable with minimal degeneration of electrode performance for extended cell stimulation, and the 3D multielectrode configuration provides a larger electrochemical surface area to augment coupling with the developing electrogenic tissue. The minor degeneration of electrode performance may be related to delamination and fractures with ageing under intense stimulation conditions, and/or decreasing conductivity with a loss of dopant. Notwithstanding, the activity was still sufficient for required ES, with a small increase of potential required to maintain the current level.

Consistent with our previous reports for the use of our biogel for human stem cell support and differentiation [15, 16], encapsulated NSCs propagated in conventional culture plates express markers VIM and MKI67 that are indicative of stem cell self-renewal and survival [24, 25]. NSCs can be readily differentiated into early neurons and glia within 3D constructs, culminating in cell-dense tissues with prolific neurite formation throughout constructs.

Interfacing our 3D NSC-laden biogel with the pillar electrodes was a simple matter of depositing the viscous amalgam of gel and cells onto the CP arrays followed by ionic crosslinking. Ensuing functional neural tissue induction was achieved over a relatively short time, with ES clearly

associated with accelerated differentiation and maturation compared to both conventional plate-based tissue induction and unstimulated array-based tissue induction.

The relatively poor maintenance of cells at the interface of unstimulated constructs and the Matrigel-coated SU-8 insulating layer of arrays was somewhat surprising, although SU-8 does comprise, among other components, antimony salts that are potentially cytotoxic [26]. While SU-8 has not previously been described for human NSC culture, biocompatibility has been demonstrated for other cell types including rat astrocytes [27], Schwann cells and neurons, as well as human fibroblasts [28]. Notwithstanding the need to further investigate the interaction between the insulating layer and cells presently used, any putative negative effects were resolved by ES. Our findings are in keeping with other reports of the effects of ES on rate and fate determination of differentiating NSCs, including our own research, albeit it through the use of CP films for 2D planar ES rather than 3D ES of tissues presently described [10-12].

The ability to stimulate cells in 3D within our biogel is partly enabled by the latter's electrical conductivity, as determined by electrochemical characterisation and deemed to be ionic in nature. Interestingly, a larger capacitive current was measured for biogel with NSCs compared to gel without. The electrical conductance of gel components CMC and Al have previously been described, with the former displaying semi-conductive properties in hydrated state, and both able to contribute to ionic conductivity [29, 30]. Other properties of CMC and Al conducive to cell support include water solubility, antimicrobial activity, and a capacity for high water retention [29, 31]. Therefore, further to our previous reports [15, 17], by combining CMC and Al with Ag, we have devised a gel not only endowed with suitable mechano-, physico- and bio-chemical properties, but also electro-chemical properties for 3D ES of NSCs and their differentiation. Not surprisingly, biogel conductance was

increased in the presence of NSCs, consistent with literature attributing conductance of cell-containing hydrogels to cell membrane cation channels, aiding ion mobility [29].

Differentiation of NSCs, including formation of functional neural networks is sustained and very consistent in the 3D ES tissue models. Remarkably, the bicuculline-induced amplification of firing rate and spike amplitude of cells in stimulated tissues shown by calcium imaging is consistent with enhanced maturation of neural networks, which include a GABAergic neuronal population [32, 33].

While the observed effects of ES can reasonably be related to modification of cell membrane ion channel activation, in turn affecting cell cycling, as well as cell adhesion, migration and neurite outgrowth and maturation [1, 6, 9, 11, 34-36], further studies will be necessary to more specifically ascertain the exact mechanism(s) of action of ES presently described. Further studies will also explore what happens to the cells over the longer term, testing other stem cell types and variable fate determination towards application of the platform for engineering other neural and non-neural tissues. We submit that the platform will be scaleable and versatile, including the potential to fabricate 3D electrodes with more complex geometries such as cubes, spheres, pyramids, and cones, and envision it being amenable to various cell and tissue types for research and translation.

Experimental Section

Human NSC culture: Human NSCs (Millipore: SCC008) were approved for use by the University of Wollongong's Human Research Ethics Committee (HE14/049). Working stocks of NSCs were maintained as adherent monolayer cultures, initially seeded at a density of 9.6 x 10^4 cells per well onto laminin (10 µg/mL in phosphate buffered saline [PBS], pH7.4; Sigma-Aldrich) coated 6-well

plates (Corning) containing 2 mL per well Complete NeuroCult Proliferation Medium (consisting of NeuroCult NS-A Basal Medium and NeuroCult NS-A Proliferation Supplement; Human; STEMCELL Technologies), and further supplemented with heparin (2 µg/mL; Sigma-Aldrich), epidermal growth factor (EGF, 20 ng/mL; Peprotech) and basic fibroblast growth factor (bFGF, 20 ng/mL; Peprotech). Cell cultures were maintained in a 5% CO_2 humidified incubator at 37°C, and culture medium was refreshed every 2-3 days with half-volume medium changes.

NSCs were passaged for subculture every 5-7 days by digesting in TrypLE Select (0.5 mL; Gibco, Life Technologies) for 3 min in a 5% CO_2 humidified incubator at 37°C. Digested cultures were triturated to single cells following addition of pre-warmed culture medium, centrifuged at 190 x g for 3 min, re-suspended in fresh pre-warmed culture medium, and re-plated as above.

Materials for printed polymer electrode arrays: 25.4 mm × 3" × 76.2 mm x 1.1 mm Titanium (~40 nm) / Au (50 nm) coated microscope slides were purchased from Deposition Research Lab, Inc. (DRLI). AZ® nLOF 2070 negative photoresist was purchased from Microchemicals and SU-8 2075 negative photoresist from MicroChem. The SU-8 was diluted with cyclopentanone to yield SU-8 2002 for thinner films. A PDMS elastomer kit (SLYGARD 184) was purchased from Dow Corning. The medical grade silicone adhesive (4100 RTV) and the conductive silver epoxy (8331 extreme conductivity grade) were purchased from Silbione and MG Chemicals respectively. 3,4-Ethylenedioxythiophene (EDOT) was purchased from AK Scientific, PEDOT:PSS (conductive grade, 1.3 wt% dispersion in H_2O); (3-Glycidyloxypropyl) trimethoxysilane (GOPS), poly (sodium 4-styrenesulfonate) (PSS) (*Mw* ~ 70000), potassium iodide (KI), iodine (I_2) and PBS tablet were purchased from Sigma-Aldrich.

Photolithography: The individually addressable Au electrodes were patterned as we have previously reported [23], by traditional photolithography technique, including the patterning of an insulating layer (Figure S1, Supporting Information). Briefly, a thin layer of AZ® nLOF 2070 negative photoresist was patterned by ultraviolet (UV) light through a mask on top of the Au layer (Figure S1a-c, Supporting Information). The unprotected Au and Ti were etched away by a KI/I_2 wet etching solution ($KI : I_2 : H_2O$ = 4g : 1g : 40 mL for the Au) followed by a 50 vol% HCl (aqueous) at 65 ^{o}C (for the Ti) (Figure S1d, Supporting Information). The photoresist was then washed away with acetone (Figure S1e, Supporting Information), rinsed with isopropyl alcohol, and dried with N_2. The SU-8 insulating layer was patterned with another mask that was carefully aligned using the mask aligner. After UV exposure and propylene glycol monomethyl ether acetate (PGMEA) development, the insulating layer was patterned on top of the patterned Au electrodes (Figure S1f-g, Supporting Information). The slides were finally cleaned with Milli-Q®, 18.2 $\mathrm{M\Omega \cdot cm}$, isopropyl alcohol and dried by N_2.

Each working electrode area comprised 36 individually addressable microelectrodes in a 6 x 6 array format (Figure 1b and 2a; Figure S2, Supporting Information). The covered insulating layer had 20 µm diameter openings to expose corresponding areas of the underlying patterned Au electrodes where CP pillars were printed (Figure S2a,b, Supporting Information; Figure 2b). The distance between electrodes was 100 µm. Each Au electrode was linked to a larger square connection point for further connection to the standard PCB pins (Figure 2c-d).

Assembly of electrode arrays: Standard PCB Connection pins with a pin distance of 2.54 mm were mounted using a pin holder (laser cut PMMA structure) and bonded to the substrate by conducting silver epoxy (extreme conductivity grade, MG. Chemicals) to diminish the contact resistance (Figure

1c; Figure S2e, Supplementary Information). PDMS chambers, fabricated by drop casting using a PMMA mold, were then bonded to the substrate by a medical grade silicone adhesive (Figure 1c; Figure S2e, Supplementary Information). A counter electrode was prepared from platinum mesh for even distribution of ES (Figure S2f, Supplementary Information). The mesh was affixed to a lid that was printed from biocompatible MED610 (Stratasys Ltd) so as to be slightly smaller than the PDMS wells' inner dimensions.

Electropolymerization of CP films: A mixed solution containing 0.01 M EDOT monomer and 0.1 M NaPSS dopant in deionized water (Milli-Q® 18.2 MΩ·cm) was used for the electropolymerization of PEDOT films. The NaPSS aqueous solution was pre degassed in N_2 for 20 min followed by addition of EDOT. Electropolymerization was carried out by potentiostatic technique at a fixed potential of 0.9 V (*vs*. Ag/AgCl (3 M KCl)). A constant charge density threshold of 115 mC/cm^2 was employed to terminate the polymer deposition. Each electrode in the MEA was electropolymerized separately for repeatability. There was a clear colour change of the electrodes from gold to dark blue before and after electropolymerization (Figure S2c, Supplementary Information).

Direct-write printing of CP pillars: Direct-write printing of CP pillars was performed as previously reported by us [18], with the difference that the 'pillars' were printed here on individually addressable electrodes (Figure 1a-c; Figure S1 and S2d, Supplementary Information). Briefly, a solution of 500 µL PEDOT:PSS (1.3 wt% dispersed in water), 175 µL DMSO and 10 µL cross-linking agent GOPS was used as the "ink" and ultrasonicated for 10 min every time before "writing" to evenly disperse the polymer. Ink was injected into a micropipette and fabricated from single barrel borosilicate capillaries using a laser puller P-2000 (Sutter Instrument). The tip diameter of the micropipette was ~ 15 µm, and slightly smaller than the diameter of the Au microelectrodes. The micropipette was

precisely positioned over the Au electrode using a Scanning Ion Conductance Microscope (SICM) system [37-39]. Once the meniscus of the "ink" at the tip of the pipette established contact with the substrate, the micropipette was raised 2 µm/s by the programmed LabVIEW software to allow the evaporation of solvents and formation of CP pillars (Figure 1f). The height and diameter of the pillars used in this study were 80 ± 2 µm and 14 ± 1 µm, respectively.

Electrochemical characterisation of printed CP pillars: Electrochemical properties of CP pillars were compared with electropolymerized CP films and bare gold microelectrodes [18]. The electrodes were characterized for cathodic charge storage capacity (CSC_C) using cyclic voltammetry (CV), charge injection limit (CIL) using voltage transient measurements (VTM), and impedance using electrochemical impedance spectroscopy (EIS). CV, VTM and EIS measurements were performed using a three-electrode setup with the tested microelectrode as the working electrode, a platinum wire as the counter electrode, and an Ag/AgCl electrode in 3 M KCl as the reference electrode. A Biologic VSP-300 electrochemical workstation was used for the measurements and each microelectrode was tested independently. It is important to note that the calculations of CSC and CIL were based on the nominal geometrical surface area of the Au microelectrodes (D = 20 µm), rather than the actual surface area of CPs.

Briefly, CVs were performed in PBS buffer from -0.9 V to 0.6 V with a scan rate of 100 mV/s. CSC_C was calculated as the time integral of the cathodic current, which indicated the charge available for stimulation under a slow potential scan (50 - 500 mV/s). The impedance was measured with a sinusoidal excitation signal of 10 mV in a frequency range of 1 Hz - 1 MHz. For VTM, a biphasic, charge balanced rectangular current pulse of 1 ms/phase, and a frequency of 50 Hz was applied. The injected current density was increased until the measured voltage drop at the electrode/electrolyte

interface reached the aqueous electrolyte potential window of -0.9 V *vs* Ag/AgCl. An accelerated ageing stability study was also performed by continuously applying 1×10^6 current pulses to the microelectrodes with a current density of 9.42 µA per phase per electrode. The phase width and pulse frequency were as described for VTM studies. The VSP-300 was programmed to perform EIS at 4 intervals during the stimulation experiment at pulse numbers 2.5×10^5, 5×10^5, 7.5×10^5 and 1×10^6 to monitor impedance and indicate whether coating delamination or damage had occurred. Delamination was deemed to occur when the % change in impedance magnitude at 100 Hz ($|Z|_{100Hz}$) exceeded 100%, indicating coating failure. Finally, the stability of CP pillar electrodes was further evaluated by performing a long-term stability test through immersion of the electrodes into PBS buffer and Neuro Basal Media (NBM; Gibco, Life Technologies) for 19 days and the EIS was recorded every 3 days. The PBS buffer and NBM were frequently refreshed.

Preparation of electrode arrays and counter electrode for cell culture: Electrode arrays were plasma treated for 2 min (Harrick Plasma Cleaner) and washed three times for 10 min with Milli-Q®, 18.2 MΩ·cm, followed by 20 min incubation with 70% (v/v) ethanol, air dried under sterile conditions, before exposure to UV light for 20 min. The surface of an electrode array was prepared by coating with Matrigel (Corning) in DMEM overnight at 4°C, and then washed with DMEM. Similarly, the counter electrode was washed with Milli-Q water, and sterilized by incubation with 70% ethanol, air dried, and exposed to UV light under sterile conditions, followed by a 1 hr incubation in DMEM before use.

Human NSC-laden biogel preparation: The biogel was prepared as previously described under sterile conditions [15-17]. Briefly, 1.5% (w/v) agarose (Ag; low gelling temperature; Sigma Aldrich) in PBS was prepared by microwave heating in a sterile 20 mL glass vial for 5 sec. The solution was

cooled briefly to allow bubbles to disperse and microwave heating repeated for 2 sec, 5 - 8 times until the agarose completely dissolved. The solution was then mixed at 60^{o}C using a magnetic stirrer, followed by addition of carboxymethyl-chitosan (CMC; Santa Cruz) powder for 5% (w/v) concentration and mixed at 60^{o}C to dissolve. Alginate (Al; MW ~50,000 Da, M/G ratio of 1.67, viscosity of 100–300 cP for 2% [w/v] solution in H_2O at 25°C; Sigma-Aldrich) powder was then added for 5% (w/v) concentration. After 1 hr stirring at 60°C, the fully dissolved final solution was cooled to 37^{o}C and 5 x 10^{6} NSCs (collected by TrypLE digestion as described previously) were added per 0.5 mL biogel solution. Cell-laden biogel was immediately deposited by pre-wetting pipetting technique using an air displacement pipette into wells of 24 well culture plates (10 µL per well; for conventional plate-based studies) or onto MEAs (10 µL per array; for stimulation studies), crosslinked using 2% (w/v) calcium chloride (0.5 mL per well; 1 mL per PDMS chamber per array) for 10 min, followed by 3 x 1 min washes at room temperature (RT) and 2 x 10 min washes in Dulbecco's Modified Eagle Medium (DMEM; Gibco, Life Technologies) in a 5% CO_2 humidified incubator at 37°C. DMEM was then replaced with Complete NeuroCult Proliferation Medium, and incubated for 1 hr, ahead of addition of fresh medium and further incubation for 3 days.

Electrochemical characterisation of biogel: Cyclic voltammetry (CV) was performed in a two-electrode configuration, and recorded using a potentiostat (CHI650e, CH Instruments). Two platinum wires were separated by a distance of ~ 3 mm and served as working and counter electrodes. The wires were inserted into biogel containing NSCs or biogel alone. As per the electrostimulation setup, all experiments were performed in DMEM, and compared to DMEM alone in the absence of biogel. Measurements were performed at a scan rate of 100 mVs^{-1} over the potential range of -0.6 to +0.6 V.

Neural tissue induction: Neural tissue induction of human NSC-laden biogels was performed by replacing NSC culture medium on the fourth day of culture with neural differentiation medium comprising DMEM/Ham's F-12 Nutrient Mixture (F-12) : Neurobasal Medium, 1:1 (v/v) (Gibco, Life Technologies) supplemented with 1% NeuroCult SMI neuronal supplement (STEMCELL Technologies), 0.5% N2 supplement (STEMCELL Technologies), 2 mM L-glutamine (Gibco, Life Technologies) and brain-derived neurotrophic factor (BDNF; 50 ng/mL; Peprotech). Differentiation of conventional plate-based and unstimulated array-based cell-laden biogels were performed over 7 days, with half-volume medium changes every 2 days.

Electrical stimulation: ES was performed for 3 days concomitantly with human NSC differentiation by applying a previously described stimulation regimen [10]. Briefly, after initial culture of NSC-laden biogel constructs for 3 days in NSC proliferation medium followed by 4 days in differentiation medium, differentiating constructs were stimulated for 8 hr per 24 hr period for 3 days in a 5% CO_2 humidified incubator at 37°C. ES was performed through a two-electrode setup, whereby the auxiliary platinum mesh electrode was submerged into the media at the top of each PDMS chamber, and the Au electrodes with printed PEDOT:PSS pillars functioning as the working electrodes. To distribute ES across all 36 PEDOT:PSS micropillars, connection pins were joined using copper tape. The constructs were stimulated at 0.25 mA per cm^2 using a biphasic waveform of 100 µs pulses with 20 µs interphase open circuit potential and a 3.78 ms short circuit (250Hz) using an A310 Accupulser Pulse Generator equipped with an A365 Isolator unit (World Precision Instruments) and interfaced with an e-corder system (eDAQ) to record resultant voltage waveforms.

Immunocytochemistry and analysis: Samples were fixed with 3.7% paraformaldehyde in PBS for 30 min at RT. Samples were then blocked and permeabilized with 5% (v/v) goat serum (Sigma-Aldrich)

in PBS containing 0.3% (v/v) Triton X-100 (Sigma-Aldrich) for 4 hr at RT. Samples were subsequently incubated with primary antibodies against vimentin (VIM; chicken; Millipore), MKI67 (mouse; Abcam), synaptophysin (SYP; rabbit; Millipore), MAP2 (mouse; Millipore), TUBB3 (chicken; Millipore), and GFAP (rabbit;, Millipore) at 4 °C overnight. On the second day, samples were rinsed 3x with 0.1% Triton X-100 in PBS and samples were incubated with species-specific Alexa Fluor conjugated secondary antibody (Life Technologies) for 2 hr at RT. Nuclei were labelled with 4',6-diamidino-2-phenylindole, dihydrochloride (DAPI; Invitrogen, Molecular Probes) at RT for 10 min. Samples were immersed in PBS and imaged with a Leica TCS SP5 II confocal microscope. Images were collected and analysed using Leica Application Suite AF (LAS AF) software and Fiji (Image J)[40]. Integrated Density (IntDen; product of mean gray value and area) was measured for 10 random regions of interest (ROI) and corrected for background IntDen. Colocalisation analysis was performed using JACoP (Just Another Colocalization Plugin)[41] to determine spatial correlation between images based on Pearson correlation coefficient.

Live-cell calcium imaging: Samples were incubated with 2 µM Fluo-4 AM (Life Technologies) in fresh neural differentiation culture medium for 60 min at 37 ^{o}C, followed by washing in 4-(2-hydroxyethyl)-1-piperazineethanesulfonic acid (HEPES) buffered Hank's balanced salt solution (HEPES-HBSS; 137 mM NaCl, 5.4 mM KCl, 1.5 mM $CaCl_2$, 0.44 mM KH_2PO_4, 0.5 mM $MgCl_2$, 0.4 nM $MgSO_4$, 0.3 mM Na_2HPO_4, 4 mM $NaHCO_3$, 5.6 mM D-glucose and 10 mM HEPES, pH 7.4). After 30 min, spontaneous intracellular calcium surges were imaged by confocal microscopy. To potentiate intracellular calcium flux, GABA(A) receptor antagonist bicuculline (50 µM; Sigma-Aldrich) was added to HEPES-HBSS for 3 min followed by further imaging. The samples were imaged with a Leica TCS SP5 II confocal microscope using LAS AF (Leica) software. Images were collected at 2 sec intervals over a

period of 150 sec, and quantified using Fiji (Image J). For each sample, 80 cells were selected and defined as ROI. Fluorescence intensity (mean grey value, F) per ROI over the time series was corrected for background intensity (F_0) at each corresponding time point. For each ROI during the time series, the change in fluorescence response was then normalised to the maximum response ($\Delta F/F_{max}$). Representative data of 4 ROI is shown.

Statistical analysis: All statistical analyses were performed in OriginPro 2015 using two-way ANOVA with Bonferroni`s post-hoc test. Homogeneity of variance tests (Brown-Forsythe Test) were performed to confirm the statistical assumptions for ANOVA were satisfied. Where homogeneity of variance was met ($P > 0.05$), statistical significance of ANOVA was set at $P < 0.05$, whereas failure to satisfy equal variance ($P < 0.05$) required increased stringency of ANOVA with statistical significance set at $P < 0.01$. Correlation analyses were performed using Pearson correlation coefficient (JACoP plugin, Fiji)[41]. Data are expressed as means ± S.D. and statistical analyses are detailed in the figure legends. No statistical methods were used to predetermine sample sizes, and experiments were replicated to appropriately reduce confidence intervals and prevent errors in statistical testing. The collection and analysis of data was carried out unblinded to the conditions of experiments, with randomisation of study samples not performed. No exclusions were made.

Acknowledgments

JMC, ETC, JH and JTS conceived the study. JMC and ETC designed the ES experiments, and ETC performed the experiments with support from AH and HK. PZ produced the electrode arrays that were characterized by PZ and ZA with support from DS. CYL assisted ETC with electrochemical characterization of the biogel, and SB manufactured the Pt counter electrodes. JMC drafted the

paper with input from ETC, PZ, JTS, CYL and AH, and all authors read, commented on, and approved the submitted paper. ETC and PZ contributed equally to the paper. The authors wish to acknowledge funding from the Australian Research Council (ARC) Centre of Excellence Scheme (CE140100012), the MacDiarmid Institute for Advanced Materials and Nanotechnology, and support of the Australian National Fabrication Facility – Materials Node. Professor Gordon Wallace acknowledges the support of the ARC through an ARC Laureate Fellowship (FL110100196).

Received: ((will be filled in by the editorial staff))

Revised: ((will be filled in by the editorial staff))

Published online: ((will be filled in by the editorial staff))

Conflict of Interest

The authors have no financial/commercial conflict of interest.

References

[1] M. Bjorninen, S. Haimi, M. J. Higgins, J. M. Crook, in *Conductive Polymers: Electrical Interactions in Cell Biology and Medicine*

Vol. Conductive Polymers Electrical Interactions in Cell Biology and Medicine

(Eds: Z. Zhang, M. Rouabhia, S. E. Moulton), CRC Press, Boca Raton, FL 2017, 347.

[2] J. M. Murbach, S. Currlin, A. Widener, Y. Tong, S. Chhatre, V. Subramanian, D. C. Martin, B. N. Johnson, K. J. Otto, MRS Communications 2018, 8, 1043.

[3] N. Zhang, F. Stauffer, B. R. Simona, F. Zhang, Z. M. Zhang, N. P. Huang, J. Voros, Biosens Bioelectron 2018, 112, 149.

[4] M. E. Mycielska, M. B. Djamgoz, J Cell Sci 2004, 117, 1631.

[5] J. F. Feng, J. Liu, L. Zhang, J. Y. Jiang, M. Russell, B. G. Lyeth, J. A. Nolta, M. Zhao, Stem Cell Reports 2017, 9, 177.
[6] J. F. Feng, J. Liu, X. Z. Zhang, L. Zhang, J. Y. Jiang, J. Nolta, M. Zhao, Stem Cells 2012, 30, 349.
[7] S. D. McCullen, J. P. McQuilling, R. M. Grossfeld, J. L. Lubischer, L. I. Clarke, E. G. Loboa, Tissue Eng Part C Methods 2010, 16, 1377.
[8] A. M. Wan, S. Inal, T. Williams, K. Wang, P. Leleux, L. Estevez, E. P. Giannelis, C. Fischbach, G. G. Malliaras, D. Gourdon, J Mater Chem B 2015, 3, 5040.
[9] M. Yamada, K. Tanemura, S. Okada, A. Iwanami, M. Nakamura, H. Mizuno, M. Ozawa, R. Ohyama-Goto, N. Kitamura, M. Kawano, K. Tan-Takeuchi, C. Ohtsuka, A. Miyawaki, A. Takashima, M. Ogawa, Y. Toyama, H. Okano, T. Kondo, Stem Cells 2007, 25, 562.
[10] E. Stewart, N. R. Kobayashi, M. J. Higgins, A. F. Quigley, S. Jamali, S. E. Moulton, R. M. Kapsa, G. G. Wallace, J. M. Crook, Tissue Eng Part C Methods 2015, 21, 385.
[11] K. A. Chang, J. W. Kim, J. A. Kim, S. E. Lee, S. Kim, W. H. Suh, H. S. Kim, S. Kwon, S. J. Kim, Y. H. Suh, PLoS One 2011, 6, e18738.
[12] L. J. Kobelt, A. E. Wilkinson, A. M. McCormick, R. K. Willits, N. D. Leipzig, Ann Biomed Eng 2014, 42, 2164.
[13] Q. Zhang, S. Beirne, K. Shu, D. Esrafilzadeh, X. F. Huang, G. G. Wallace, Sci Rep 2018, 8, 9855.
[14] R. Donato, E. A. Miljan, S. J. Hines, S. Aouabdi, K. Pollock, S. Patel, F. A. Edwards, J. D. Sinden, BMC Neurosci 2007, 8, 36.
[15] Q. Gu, E. Tomaskovic-Crook, R. Lozano, Y. Chen, R. M. Kapsa, Q. Zhou, G. G. Wallace, J. M. Crook, Adv Healthc Mater 2016, 5, 1429.
[16] Q. Gu, E. Tomaskovic-Crook, G. G. Wallace, J. M. Crook, Methods Mol Biol 2018, 1758, 129.
[17] Q. Gu, E. Tomaskovic-Crook, G. G. Wallace, J. M. Crook, Adv Healthc Mater 2017, 6.
[18] P. Zhang, N. Aydemir, M. Alkaisi, D. E. Williams, J. Travas-Sejdic, ACS Appl Mater Interfaces 2018, 10, 11888.
[19] D. R. Merrill, M. Bikson, J. G. Jefferys, J Neurosci Methods 2005, 141, 171.
[20] Z. Wang, J. Xu, Y. Yao, L. Zhang, Y. Wen, H. Song, D. Zhu, Sensors and Actuators B: Chemical 2014, 196, 357.
[21] D. A. Mengistie, P.-C. Wang, C.-H. Chu, J. Mater. Chem. A, 2013, 1, 9907.
[22] Y. H. Kim, C. Sachse, M. L. Machala, C. May, L. Müller‐Meskamp, K. Leo, Advanced Functional Materials 2011, 21, 1076.
[23] Z. Aqrawe, B. Wright, N. Patel, Y. Vyas, J. Malmstrom, J. M. Montgomery, D. Williams, J. Travas-Sejdic, D. Svirskis, Sensors and Actuators B: Chemical 2019, 281, 549.
[24] D. Park, A. P. Xiang, F. F. Mao, L. Zhang, C. G. Di, X. M. Liu, Y. Shao, B. F. Ma, J. H. Lee, K. S. Ha, N. Walton, B. T. Lahn, Stem Cells 2010, 28, 2162.
[25] L. H. Pevny, S. K. Nicolis, Int J Biochem Cell Biol 2010, 42, 421.
[26] K. V. Nemani, K. L. Moodie, J. B. Brennick, A. Su, B. Gimi, Mater Sci Eng C Mater Biol Appl 2013, 33, 4453.

[27] E. S. Ereifej, S. Khan, G. Newaz, J. Zhang, G. W. Auner, P. J. VandeVord, J Biomed Mater Res A 2011, 99, 141.
[28] S.-H. Cho, H. M. Lu, L. Cauller, M. I. Romero-Ortega, J.-B. Lee, G. A. Hughes, IEEE Sensors Journal 2008, 8, 1830.
[29] G. Kaklamani, D. Kazaryan, J. Bowen, F. Iacovella, S. H. Anastasiadis, G. Deligeorgis, Regen Biomater 2018, 5, 293.
[30] C. Xu, S. Guan, S. Wang, W. Gong, T. Liu, X. Ma, C. Sun, Mater Sci Eng C Mater Biol Appl 2018, 84, 32.
[31] B. Fonseca-Santos, M. Chorilli, Mater Sci Eng C Mater Biol Appl 2017, 77, 1349.
[32] R. Tyzio, A. Represa, I. Jorquera, Y. Ben-Ari, H. Gozlan, L. Aniksztejn, J Neurosci 1999, 19, 10372.
[33] J. A. van der Linden, M. Joels, H. Karst, A. J. Juta, W. J. Wadman, Neurosci Lett 1993, 155, 230.
[34] K. R. Robinson, J Cell Biol 1985, 101, 2023.
[35] G. Thrivikraman, G. Madras, B. Basu, Biomaterials 2014, 35, 6219.
[36] J. Zhang, M. Calafiore, Q. Zeng, X. Zhang, Y. Huang, R. A. Li, W. Deng, M. Zhao, Stem Cell Rev 2011, 7, 987.
[37] C. Laslau, D. E. Williams, B. Kannan, J. Travas-Sejdic, Advanced Functional Materials 2011, 21, 4607.
[38] C. Laslau, D. E. Williams, J. Travas-Sejdic, Progress in Polymer Science 2012, 37, 1177.
[39] N. Aydemir, J. Parcell, C. Laslau, M. Nieuwoudt, D. E. Williams, J. Travas-Sejdic, Macromol Rapid Commun 2013, 34, 1296.
[40] J. Schindelin, I. Arganda-Carreras, E. Frise, V. Kaynig, M. Longair, T. Pietzsch, S. Preibisch, C. Rueden, S. Saalfeld, B. Schmid, J. Y. Tinevez, D. J. White, V. Hartenstein, K. Eliceiri, P. Tomancak, A. Cardona, Nat Methods 2012, 9, 676.
[41] S. Bolte, F. P. Cordelieres, J Microsc 2006, 224, 213.

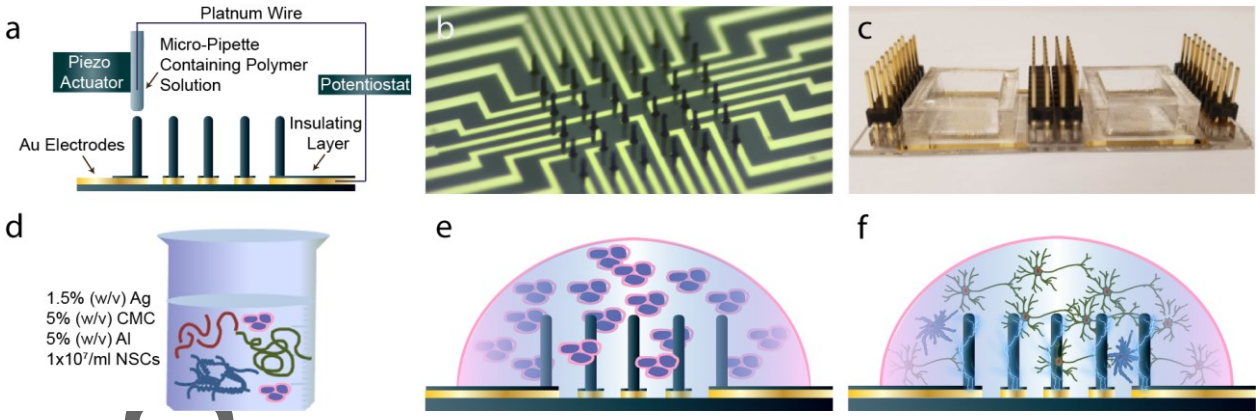

Figure 1. Schematic illustrating the assembly and use of the integrated 3D ES tissue engineering platform, including printed CP pillar MEAs with conductive cell-laden biogel to form electrogenic human neural tissues. a) Direct write printing of 3D CP pillars by scanning ion conductance microscopy (SICM). b) Printed individually addressable 3D pillar (height: 80 ± 2 µm, diameter 14 ± 1 µm) electrodes. c) Assembled 3D MEAs with connection pins and CP pillar electrodes within bonded PDMs wells. d) Preparation of conductive cell-laden biogel from Al, CMC and Ag followed by addition of human NSCs. e) Interfacing NSC-laden biogel with 3D MEAs by deposition of viscous amalgam of gel and cells onto CP arrays followed by ionic crosslinking. f) Functional 3D neural tissue induction and maturation with ES.

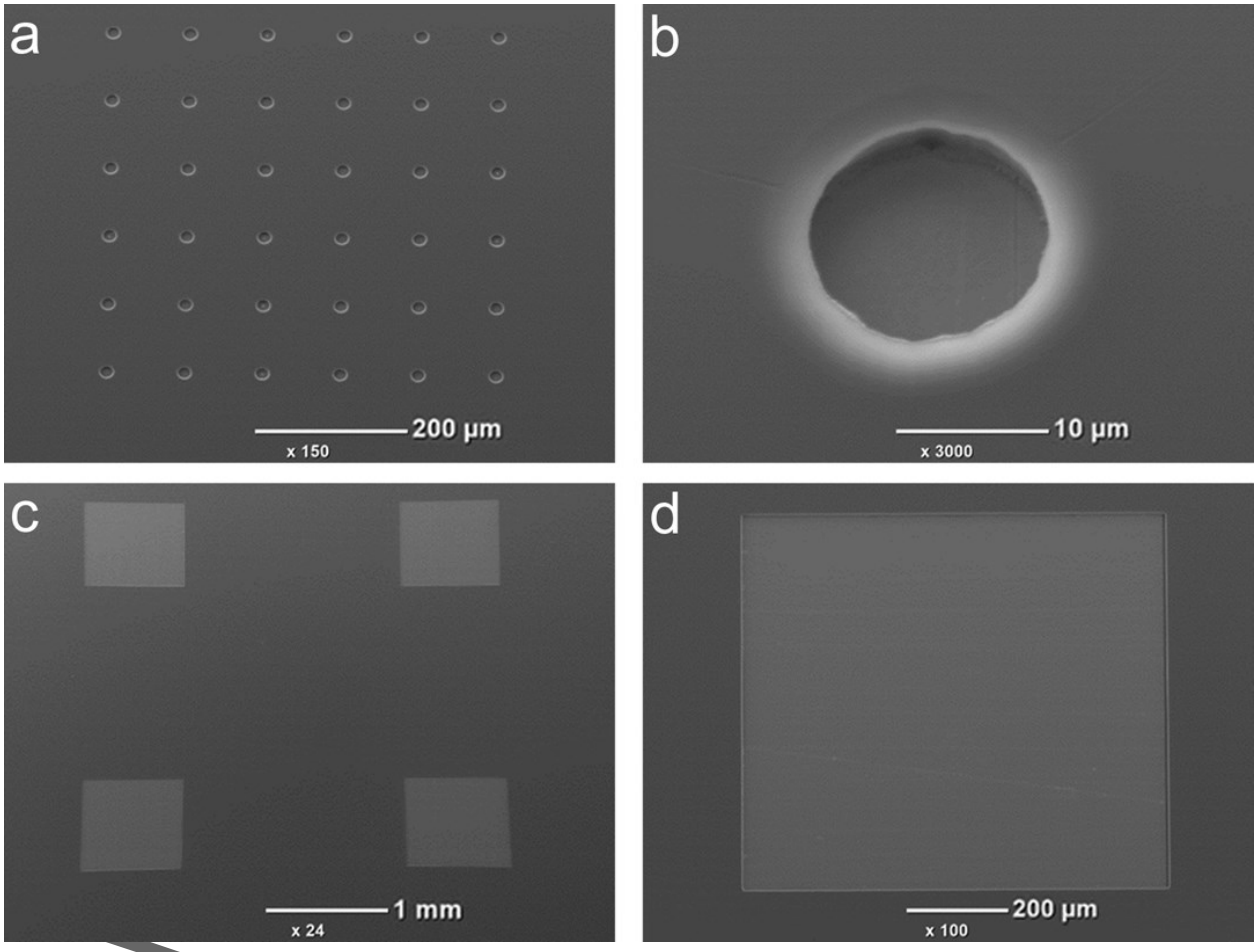

Figure 2. Scanning Electron Microscopy images of the MEAs. a) A 6 × 6 MEA for the writing of pillars. (b) An enlarged single electrode. c) Connection points for connecting standard PCB pins. d) An enlarged connection point.

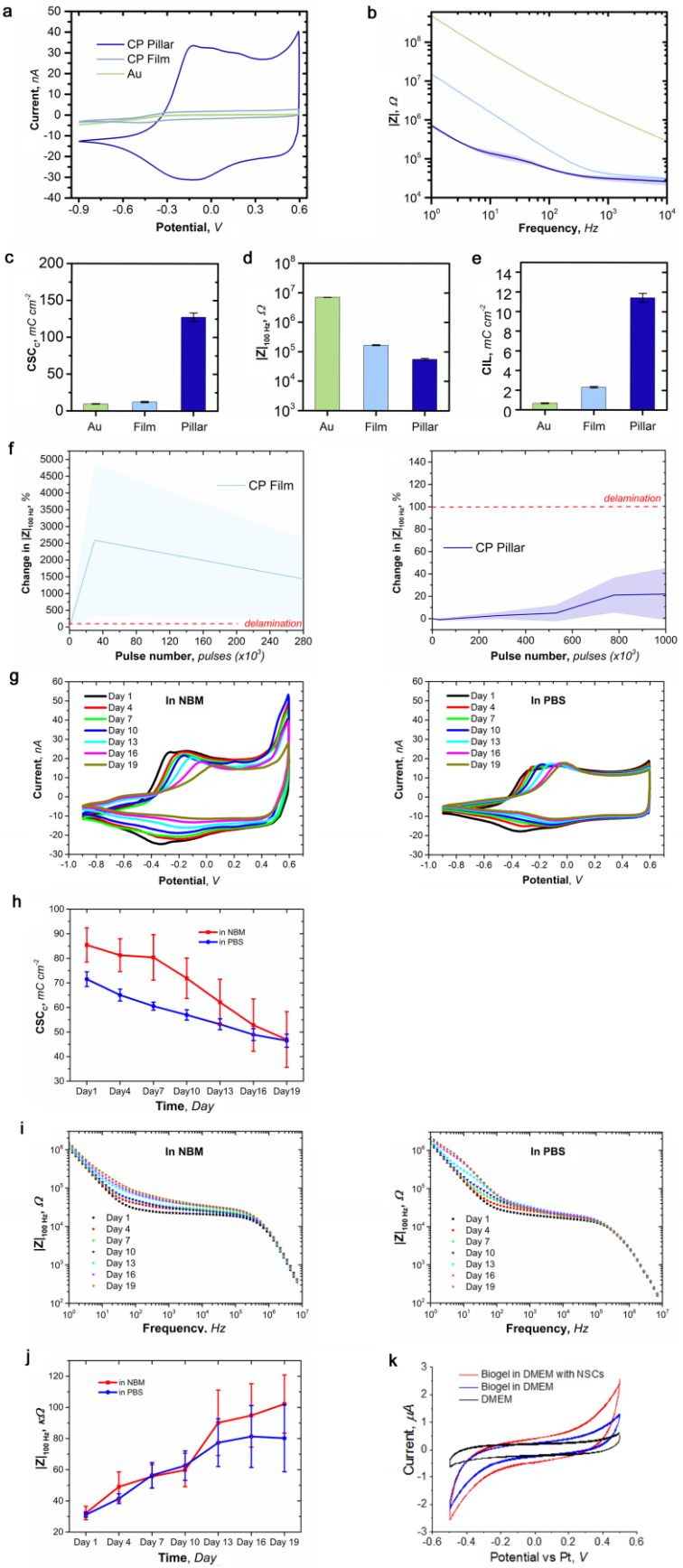

Figure 3. Electrochemical characterisation of CP pillar electrodes and biogel. a) CVs showing a large increase in capacitance for CP pillar electrodes compared to electropolymerised CP film and a Au electrode (respective controls). b) Impedance spectroscopy results displayed as a Bode plot. Impedance magnitude is lowest at all frequencies for CP pillars compared to controls. c) Cathodic charge storage capacity was highest for CP pillars compared to controls. d) Impedance magnitude at 100 Hz was lowest for CP pillar electrodes compared to controls. e) Charge injection limit was increased for CP pillars compared to controls. f) Effect of pulsed current stimulation at a frequency of 50 Hz on impedance of CP films and pillars. $|Z|_{100Hz}$ changes as a function of pulse number. Delamination was observed to occur when the change in $|Z|_{100Hz}$ exceeded 100% (red dashed lines). Data points indicate the mean and shaded sections indicate the positive standard deviation (n = 3). g) CVs of CP pillars incubated in NBM and PBS respectively showing long term electrochemical stability. h) Plot of CSC_C from the cathodic region of CV as a function of time. i) Bode plots from EIS of CP pillars in NBM and PBS. j) Plot of impedance magnitude of CP pillars at a frequency of 100 Hz as a function of time. k) CVs of human NSC-laden biogel (biogel in DMEM media with NSCs), biogel in DMEM and DMEM performed at 100 mVs-1.

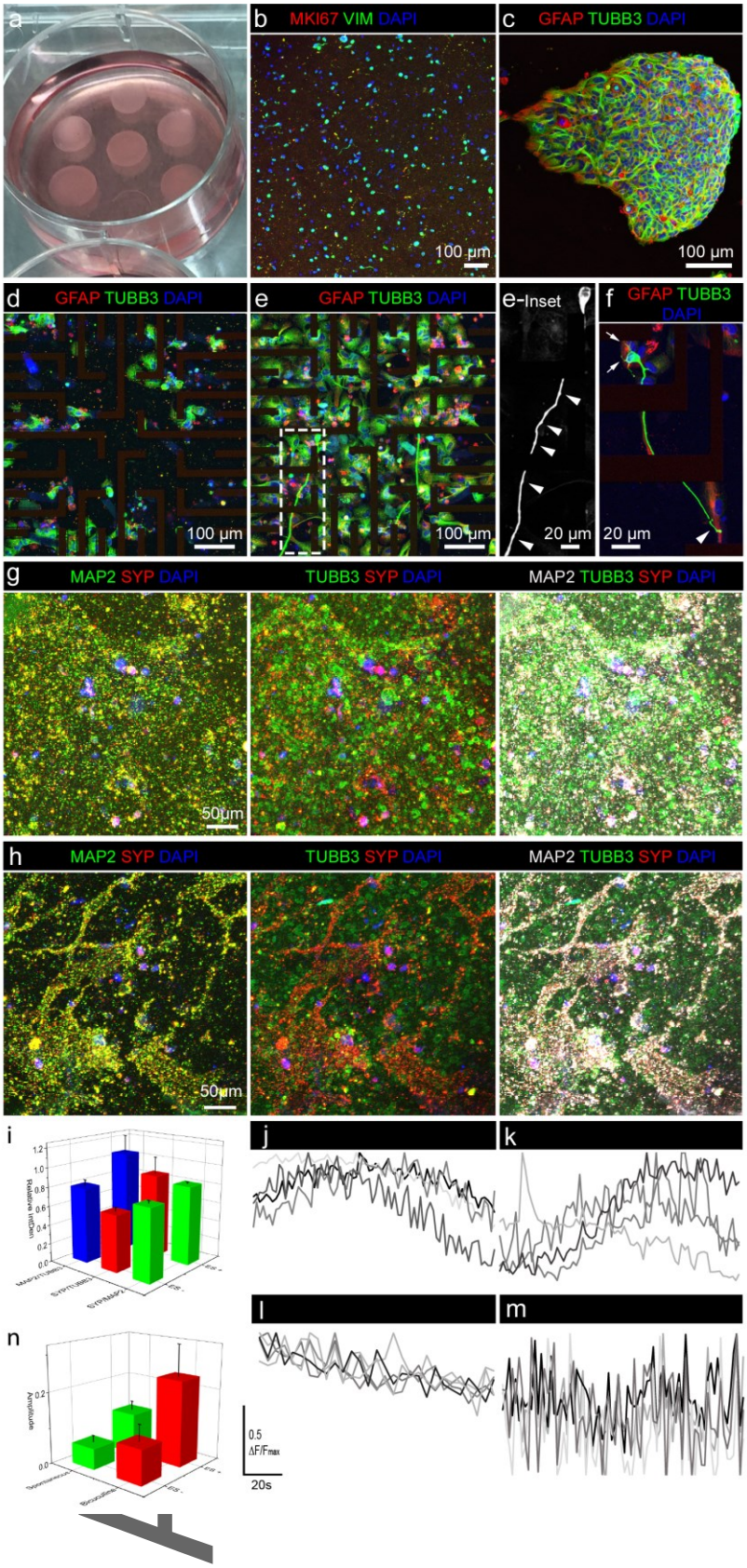

Figure 4. Human neural tissue induction under conventional plate-based culture, and on 3D MEAs with or without ES. a) Representative photograph of 3D plate-based human NSC-laden biogel constructs in a well of a standard 6-well culture plate. b,c) Immunophenotyping of 3D plate-based cell-laden biogel constructs at day 7 of human NSC culture and differentiation respectively, confirming high-density NSC encapsulation (MKI67+ and VIM+) and induction of early neuronal (TUBB3+) cells, related neurite formation, and glial (GFAP+) cells respectively. d) In situ immunophenotyping of 3D MEA-based cell-laden constructs at day 7 of human NSC differentiation without ES. The image was taken at the interface of the ventral surface of the construct and the Matrigel-coated insulating layer covering the Au electrodes and shows low-density human NSC-derived neurons (TUBB3+), related neurite formation, glial (GFAP+) cells, and underlying patterned Au electrodes apparent as dark bands/silhouettes. e) In situ immunophenotyping of 3D MEA-based cell-laden constructs at day 7 of human NSC differentiation including 3 days ES. While similar to d, the image depicts the interface of the ventral surface of the construct and the Matrigel-coated insulating layer covering the Au electrodes, induction of high-density neurons (TUBB3+), related neurite formation (including elongated axons; inset), and glial (GFAP+) cells are shown, with underlying patterned Au electrodes again apparent as dark bands/silhouettes. f) High magnification image of a 3D MEA-based immunolabelled neuron (TUBB3+) and associated glial (GFAP+) cells following 7 days of differentiation including 3 days ES, with the polarised neuron possessing dendritic arborisations (arrows) and an elongated axon with synaptic varicosities (see also e-inset arrow heads) and terminal bulbs abutting glia (arrow head). Similar to d and e, underlying patterned Au electrodes were apparent as dark bands/silhouettes. g,h) Confocal z-projections (max; ~200 µm)

of 3D MEA-based cell-laden constructs at day 7 of human NSC differentiation without (g) or with (h) 3 days ES, indicating the level and localisation of early neuronal TUBB3, mature neuronal MAP2, and synaptic vesicle protein SYP immunolabelling. Constructs with (h) ES comprised MAP2+ and SYP+ (ie. colocalized) tracts of high-density mature neuronal networks, suggestive of more structured neuronal network formation and tissue maturation compared to c and g. Quantitative immunocytochemistry-based measures of spatial colocalization of markers determined by correlation analyses showed greater colocalization of MAP2 with SYP for stimulated (r=0.748) compared to unstimulated (r=0.595) tissues, while a low spatial correlation between TUBB3 and SYP was measured for samples with (r=0.169) or without (r=0.258) ES. Pearson correlation coefficient. i) Quantitative assessment of TUBB3, MAP2 and SYP immunocytochemistry, with indices of neuronal maturation derived from ratios of mature neuronal MAP2 *vs* immature neuronal TUBB3 ($P < 0.0001$), SYP *vs* TUBB3 ($P < 0.0001$), and SYP *vs* MAP ($P > 0.05$) expression levels (Integrated Density; IntDen), indicating more mature neuronal tissue for stimulated compared to unstimulated samples. Mean ± S.D.; $n = 10$. Two-way ANOVA with Bonferrroni post hoct test. $F(5,54)=18.50$, $P < 0.001$. j-m) Live-cell calcium imaging of 3D MEA-based cell-laden constructs at day 7 of human NSC differentiation, without (j,k) or with (l,m) ES. Cells labelled with fluorescent calcium indicator Fluo-4 AM exhibited spontaneous calcium flux (j,l). Following addition of GABAA antagonist bicuculline, stimulated cells (m) exhibit elevated calcium flux with an increased firing rate and spike amplitude compared to unstimulated constructs (k). n) Quantitative analysis of live-cell calcium flux indicated a statstically significant increase in amplitude with ES. Mean ± S.D.; n = 80. Two-way ANOVA with Bonferroni post hoc test. $F(3,300)=177.7$, $P < 0.0001$.

The table of contents entry: An array of printed polymer pillar microelectrodes is interfaced with an electrically conductive biogel encapsulating human neural stem cells for 3D electrical

stimulation of developing neural tissue. Stimulation enhances tissue maturation evidenced by widespread tracts of high-density mature neurons, and functional neural networks with increased response to drug induced disinhibition. The platform is scaleable and amenable for research and translation.

Keywords: 3D electrical stimulation; human neural tissue; stem cells; conductive biogel; printed conducting polymer electrodes

*Author(s), and Corresponding Author(s)** Eva Tomaskovic-Crook, Peikai Zhang, Annika Ahtiainen, Heidi Kaisvuo, Chong-Yong Lee, Stephen Beirne, Zaid Aqrawe, Darren Svirskis, Jari Hyttinen, Gordon G Wallace, Jadranka Travas-Sejdic*, Jeremy M Crook*

Title: Human Neural Tissues from Neural Stem Cells Using Conductive Biogel and Printed Polymer Microelectrode Arrays for 3D Electrical Stimulation

ToC figure: